FEA-Based Simulation of Accelerated Ageing in a Power Cable Due to Sustained Partial Discharge Activities in a Spherical Cavity

Umar Musa[1] · Abdullahi A. Mati[1,2] · Abdullahi A. Mas'ud[3] · Gaddafi S. Shehu[1] · Johnatan M. Rodríguez-Serna[4] · Saud J. Al-Shammari[3] · Mohamad N. K. H. Rohani[5] · Firdaus Muhammad-Sukki[6,7,8]

Abstract

The reliability of electrical assets is greatly influenced by the quality of their insulations. Key power installations such as power cables are manufactured with polymer-based materials as part of their insulation system. However, accelerated ageing of equipment insulations due to manifestation of defect(s), and partial discharges (PDs) can offset the operation of these systems or even lead to breakdowns. In this study, a non-deterministic model to simulate the phenomenon of repetitive discharges in a spherical air-filled cavity within a practical power cable has been investigated. In addition, the work contributes to the understanding of PD behaviour and field distribution under different ageing conditions considering changes in cavity surface conductivity. First, a section of the practical XLPE cable containing the cavity is developed in 2D using COMSOL software, and a finite element analysis (FEA) of the electric field distribution within the cable insulation is performed. The magnitude of the cavity local field, that is enough to ignite a PD, is investigated. Alongside the COMSOL model, the activity of sustained internal PD is simulated in MATLAB by introducing a random sample generating factor and adjusting the model's parameters to obtain something close to the practical results. Furthermore, the impact of continuous PD in the power cable under different cavity dimensions and surface conductivity is likewise investigated, and a phase resolved PD (PRPD) pattern is established. The result shows that the magnitude and number of PDs per cycle increase as the cavity size and its surface conductivity increase. Finally, when the cavity surface conductivity rises, the amplitude of the electric field generated by the surface charge distribution and the number of PDs per cycle approach their maximum values.

Keywords Medium voltage · Cross-linked polyethylene cable · COMSOL and partial discharge

1 Introduction

Cross-linked polyethylene (XLPE) cables are widely acceptable variants of polymer-based power cables used in electric power grids. These cables are largely used because of their good mechanical, electrical and thermomechanical properties. In addition, the ease of installation and maintenance accord the XLPE cables added advantage, particularly for underground power transmission and distribution purposes

✉ Abdullahi A. Mas'ud
   masud_a@rcjy.edu.sa

✉ Firdaus Muhammad-Sukki
   f.muhammadsukki@napier.ac.uk

1 Department of Electrical Engineering, Ahmadu Bello University, Zaria, Nigeria

2 Centre for Energy Research and Training (CERT), Samaru, Zaria, Nigeria

3 Department of Electrical Engineering, Jubail Industrial College, Jubail, Kingdom of Saudi Arabia

4 Departamento de Ingeniería Eléctrica, Facultad de Ingeniería, Universidad de Antioquia (UdeA), Calle 67 No. 53-108, 050010 Medellín, Colombia

5 Faculty of Electrical Engineering and Technology, Universiti Malaysia Perlis, 02600 Arau, Perlis, Malaysia

6 School of Computing, Engineering and the Built Environment, Edinburgh Napier University, Merchiston

Campus, 10 Colinton Road, Edinburgh EH10 5DT, Scotland, UK

7 Razak Faculty of Technology and Informatics, Universiti Teknologi Malaysia, Jalan Sultan Yahya Petra, 54100 Kuala Lumpur, Malaysia

8 Solar Research Institute (SRI), School of Electrical Engineering, College of Engineering, Universiti Teknologi MARA (UiTM), 40450 Shah Alam, Malaysia

[1, 2]. According to earlier research, high-voltage (HV) and medium-voltage (MV) power cables account for over 11% of the entire power distribution network. For such reasons, PD studies, as it relates to power cables, has become imperative for effective and reliable operation of the overall power system [3].

Partial discharges (PDs) have been explained by researchers from varying perspectives. According to IEC 60270, PDs are stochastic events that describe a localized breakdown in insulations between electrodes [4–6]. The knowledge of PD is critical for assessing the level of degradation in insulation systems of HV plants as its emergence signifies ageing [7]. In electric power cables, PD often occurs in the insulation-defect(s) by the availability of a seed charge and sufficiently high field [8–10]. Sustained discharge activities are likely to be maintained in the defect(s) with the availability of residual charges either from past PD events or defect(s) in the wall.

The geometrical and physical properties of the discharging domain significantly influence PD behaviour [11–13]. The greatest physical property that impacts PD is the local electric stress as its magnitude affects the ignition and extinction of the PD phenomenon [14]. In a cavity-defect, the size and entrapped gaseous composition, mostly from manufacturing imperfections, influence the discharge parameters. For example, the rate of discharge among other PD associated parameters is highly dependent upon the cavity size [14, 15].

When in service, power cables are usually subjected to high and continuous electrical excitation [16, 17]. This excitation, in turn, ensures constant external fields in the insulation bulk, capable of sustaining an ongoing discharge phenomenon within the cavity. The result of such a process is a rapid erosion and degradation of the insulation system, finally leading to the cable's complete failure [17, 18]. Replacing a failed cable in power grid can last up to a few hours or days, and during this period the affected areas are subjected to blackout. Preventive actions such as condition monitoring of the facility will go a long way in improving the overall system resiliency. A critical diagnostic tool used for assessing HV installations is PD [19–22]. PDs are both a cause and a consequence of dielectric ageing, activating one of the quicker degradation processes in solid polymeric dielectrics like XLPE [23–25]. The changes on the behaviour of PDs characteristics, such as the φ–q–n patterns, q_{max}, q_{mean}, q_{min}, among others during ageing, can be correlated with the variations on the cavity surface [26, 27]. The pressure and gas composition, and the inception of trees [28], can be used for implementing diagnosis and prognosis analyses. The φ–q–n patterns are also known as PRPD patterns, which corresponds to a graphical representation, in 2d or 3d, of the distribution in phase of the PD pulses, magnitudes and rate, taking as reference a period of the sinusoidal wave of the applied voltage. They present particular distributions depending on the PD source. Some authors have proposed life models and health indexes based on the characteristics of PD behaviour in simulations and measurements [23, 24, 29]. Thus, an in-depth understanding of sustained discharge activities is critical for the analysis and interpretation of PD severity in the equipment.

Prognosis of sustained PD activities in HV apparatus, based on tests, are at an advanced stage [30–33]. However, the case is different through simulation as only a few PD parameters can only be obtained by measurements. This scenario has made it difficult to investigate the physical processes of PD in a cavity from modelling perspective. To this moment, handful of models aimed at simulating PD in an insulation-cavity have been proposed in the literature [18, 34–37]. Although all models, to some extent, have provided appropriate insights into the behaviour of PD, the FEA-based PD models have proven to be more accurate [38]. This model utilizes a number of experimentally determined physical parameters to explain the behaviour of sustained PD in systems. Section 2.2 summarizes the current state of the art for models for simulating PDs in cavities within solid dielectrics.

In this paper, a computer simulation model of PD activity in a single-core, 11 kV, XLPE power cable containing a cavity is presented. In addition, simulation results of sustained PD activity and electric field distribution, considering different cavity sizes and changes in the surface conductivity, due to the PD induced ageing, are presented. This paper is organized as follows: after the introductory part, already presented at Sect. 1, the theoretical background of the PD modelling is presented in Sect. 2; then, the results and discussion with the case study are presented in Sects. 3 and 4, respectively, and lastly, some conclusions and future work are depicted in Sect. 5.

2 FEA PD Modelling

PDs are a phenomenon that has been modelled using several approaches, the key difference being how the electric field created by prior PDs is modelled [5]. In FEA models, the electric fields are calculated by solving the partial differential equations in the domains of interest using the conductance and electrostatic models [8, 9]. Below, the modelling process in FEA of PDs in gaseous cavities within the solid dielectric is described in detail.

2.1 Multiphysics Model for Field Calculation

For a non-dispersive, bounded, homogenous and isotropic material, the basic field equations that describe the behaviour of electric field variables (electric scalar potential and field

strength) are derived from the well-known Maxwell's equations as follows [3, 11]:

$$\vec{D} \;=\; \varepsilon\,\vec{E} \;=\; -\varepsilon\,\nabla U \tag{1}$$

$$\vec{J} \;=\; \sigma\,\vec{E} \;=\; -\sigma\,\nabla U \tag{2}$$

$$\nabla \cdot \left(-\sigma\,\nabla U \;-\; \frac{\partial}{\partial t}\varepsilon_0\varepsilon_r\nabla U \right) = 0 \tag{3}$$

where $\vec{E}$ is the electric field strength, $\vec{D}$ is the electric field displacement, σ is electric conductivity, $\vec{J}$ represents the free current density, $\varepsilon_0\varepsilon_r$ represent the relative and vacuum permittivity of the insulation system, and U denotes the general location's scalar potential.

2.2 Stochastic Model for PD Calculation

For the sake of completeness, the evolution of PD simulation models, in cavities within solid insulation, is considered in the first part of this section, after which the theoretical framework of the PD model used for simulation is presented.

The analytical model is based on the electromagnetic theory and some considerations that, under practical conditions, are valid [39]. A generalization of the analytical model was presented in [8] to simulate PDs in cavities and protrusions and has been utilized to obtain the theoretical magnitude of PD charge within insulated cables [40]. In [41], the analytical model was used to study the characteristics of PDs under direct current (DC) voltage. Deterministic variations of analytical models for PD have also been proposed that can approximately represent the PD charge magnitudes. However, they are unable to reproduce the phase distribution of PD pulses that have been found experimentally [42, 43]. Although the analytical stochastic models show good results when compared to experimental measurements, they do not consider all the physical processes and phenomena involved during PD, such as the memory effect, charge decay, temperature and pressure variations during and after PD activity [2]. A critical discussion of the analytical model considerations, as well as, an improved version that increases the modelling accuracy for cavities of different sizes, are presented in [10]. In [21], a multiphysics version of the analytical model was presented that allows calculating the pressure and temperature variations within the cavity subjected to sustained PD activity.

Gemant and Philippoff [44] first introduced the three-capacitance model to evaluate power losses in cables owing to PD in cavities. Later, Whitehead [34] proposed a modified equivalent circuit that is known as the "abc" model. In this model, unlike what happens in the analytical and FEA models, analysis are made as a function of currents and voltages in the equivalent capacitances' terminals, allowing the simulations to be easily implemented in a dedicated circuit and network analysis software, making this model widely used [45–49]. A variable resistance technique may also be used to represent the surface charge dynamics [50]. Nevertheless, the high non-linearity introduced into the circuit by the streamer equivalent resistance causes numerical challenges, necessitating extensive computing effort to solve the resultant circuit. In [2], a modification to the equivalent "abc" circuit presented in [51] was proposed to consider the stochasticity of the PD phenomenon and a method was proposed to calculate the equivalent capacitance of the cavity that allows to reconcile the models of capacitors and electromagnetic fields.

FEA models numerically solve the field equations in partial derivatives and has practically no limitations regarding the geometry of the test object, the waveform of the applied voltage and even the linearity or isotropy of the materials. In addition, multiple-physics can be considered; electrical, thermal and mechanical, interrelated during PD [15], the charges and currents, induced and real, are calculated numerically in the electrodes using boundary conditions and field solutions and in the cavity, without the need to use analytical expressions and electrostatic approximations. These models have been used to investigate the behaviour of PD in cavities under various frequency conditions [12, 52, 53], amplitude and waveform of the applied voltage [41, 54–56], cavity size and location [57, 58], temperature [15, 59] and number of cavities [60]. Electrostatic FEA models have been used to analyse changes in PD behaviour during the ageing process [53], and in [14] a 3D electrostatic model was used to study the PD phenomenon in a geometry similar to that found in a power cable of practical dimensions. In [5], a generalized electrostatic model for PD simulation using a surface continuous charge distribution was presented. In [61], a new hybrid model was proposed that combines the advantages of the electric current and electrostatic FEA models and allows to overcome the difficulties about the surface charge distribution of the existing electrostatic FEA models [62].

There are other advanced models in which the physical processes of impact ionization, recombination, addition, drift of charge carriers and diffusion are quantitatively defined by fluid equations to describe cavity plasma dynamics during PD [63]. In these models, the chemical and physical phenomena that occur during PD in cavities are considered in a precise and detailed manner [64]. However, the solution of these models requires high computational consumption which makes them impractical for multiple PD analysis and ageing where simulation for hundreds of cycles of the AC voltage signal is required.

Experimental studies have revealed the PD phenomenon to be non-deterministic. For a cavity containing gaseous substance, such as air, two conditions must be satisfied for PD to begin. First, the electric field strength at the cavity centre must be strong enough to ignite and maintain an avalanche (streamer inception); and then, there must be a seed electron within the cavity to kickstart the ionization process. While the magnitude of the local electric field strength can be computed from FEA, the condition about the availability of the seed electron is evaluated through a critical avalanche criterion and the electron generation rates from different sources [8].

2.2.1 The Streamer Inception and Extinction Fields

The minimum electric field strength required for initiating a streamer-type PD within a cavity, denoted as E_{inc}, depends on the cavity diameter as well as the pressure and the ionization parameters of the gas inside the cavity. Once the radius and the pressure of the gas filling the cavity are known, the inception magnitude of the electric field is obtained using the expression [8, 9]:

$$E_{inc} = p\left[1 + B\big/(2\,p\,r_{cav})^n\right](E\big/p)_{cr} \qquad (4)$$

where r_{cav} and p represent the radius and cavity pressure, respectively, and B, n and $(E/p)_{cr}$ are parameters related to the gas ionization process. For air-filled cavities: $n = 0.5$, $B = 8.6$ m$^{1/2}$.Pa$^{1/2}$ and $(E/p)_{cr} = 24.2$ V.Pa^{-1}.m^{-1} [9].

After a PD event, the electric field strength produced by the chargers left by the streamer at the cavity surface, Poisson's type field, opposes the electric field strength established by the HV source, Laplacian Field, and when its magnitude is lower than an extinction value, E_{ext}, the streamer propagation inside a discharging cavity ceases. The electric field extinction magnitude is estimated using the expression [9]:

$$E_{ext} \approx p\gamma(E\big/p)_{cr} \qquad (5)$$

where γ is a dimensionless factor that changes accordingly with variation in voltage polarity. The value of γ is usually obtained from experimental measurements.

The PD occurrence in a cavity entails increasing the value of the cavity gas conductivity. At a predefined value of conductivity, σ_{cav_max}, the intensity of the field inside the cavity reduces drastically. By maintaining the conductivity at this higher value, the cavity field recedes further, and the PD signals cease to exist at certain charge magnitude.

2.2.2 Electron Generation

Seed electrons required to initiate an avalanche and are produced by two basic processes: volume production and surface emission. In the volume electron generation process, the seed electron is assumed to emerge from ionization activities caused by background radiation in a virgin cavity. In the case of surface emission, first electrons are produced through detrapping of electrons, previously left by the PD activity, from the cavity wall [8]. Therefore, the overall electron generation rate for a specific instant of time, $N_{e,tot}(t)$, is defined as the sum of the charge generating processes caused by volume ionization, $N_{e,vol}(t)$ and surface emission, $N_{e,surf}(t)$:

Therefore, the overall electron generation rate, $N_{e,tot}(t)$, is the summation of the charge generation processes due to volume ionization, $N_{e,vol}$, and surface emission, $N_{e,surf}(t)$ [8, 9].

$$N_{e,tot}(t) = N_{e,vol}(t) + N_{e,surf}(t) \qquad (6)$$

Starting with the volume ionization process, the initial electron generation rate is computed using [9]:

$$N_{e,vol}(t) = C_{rad}\psi_{rad}(\rho\big/p)_0\,p\,\frac{4}{3}\pi r_{cav}^3\left(1 - v^{-\beta_0}\right) \qquad (7)$$

where ψ_{rad} represents the radiation quantum flux density, C_{rad} indicates the interaction between radiation and gas molecules, β_0 is an exponent in approximation for effective ionization coefficient, v is the quotient of the applied voltage, U_0, to the inception voltage, U_{inc}, and $(\rho/p)_0$ denotes the pressure reduced gas density [8].

In the surface emission process, the electron de-trapping mechanism is highly dependent on two quantities: the temperature within the cavity and the local electric field strength magnitude at the cavity centre. Niemeyer argued that the said process of charge generation obeys the Richardson–Schottky scaling and is governed by [8, 9]:

$$N_{e,surf}(t) = N_{e,det}\,v_0\exp\left\{-\left(\phi - \sqrt{eE_{cav}(t)\big/4\pi\varepsilon_0}\right)\big/k_bT\right\} \qquad (8)$$

where T represents the absolute temperature, k_b is the Boltzmann constant, v_0 is the fundamental photon frequency of insulation material, ϕ is the effective de-trapping work function, and $N_{e,det}$ is the total available charges to be de-trapped for an immediate PD event and is obtained using [9]:

$$N_{e,det} = N_{e,surf0}\exp\left(-\frac{t - t_{PD}}{\tau_{dec}}\right) \qquad (9)$$

$$N_{e,surf0} = \xi\left(\frac{q}{e}\right) \qquad (10)$$

where τ_{dec} indicates the effective time decay constant, e is the elementary charge, q is the real charge on the cavity surface after the previous PD event, t_{PD} is the time passed since

Fig. 1 Charge migration inside cavity during two PD events with **a** same **b** opposite directions of fields [31]
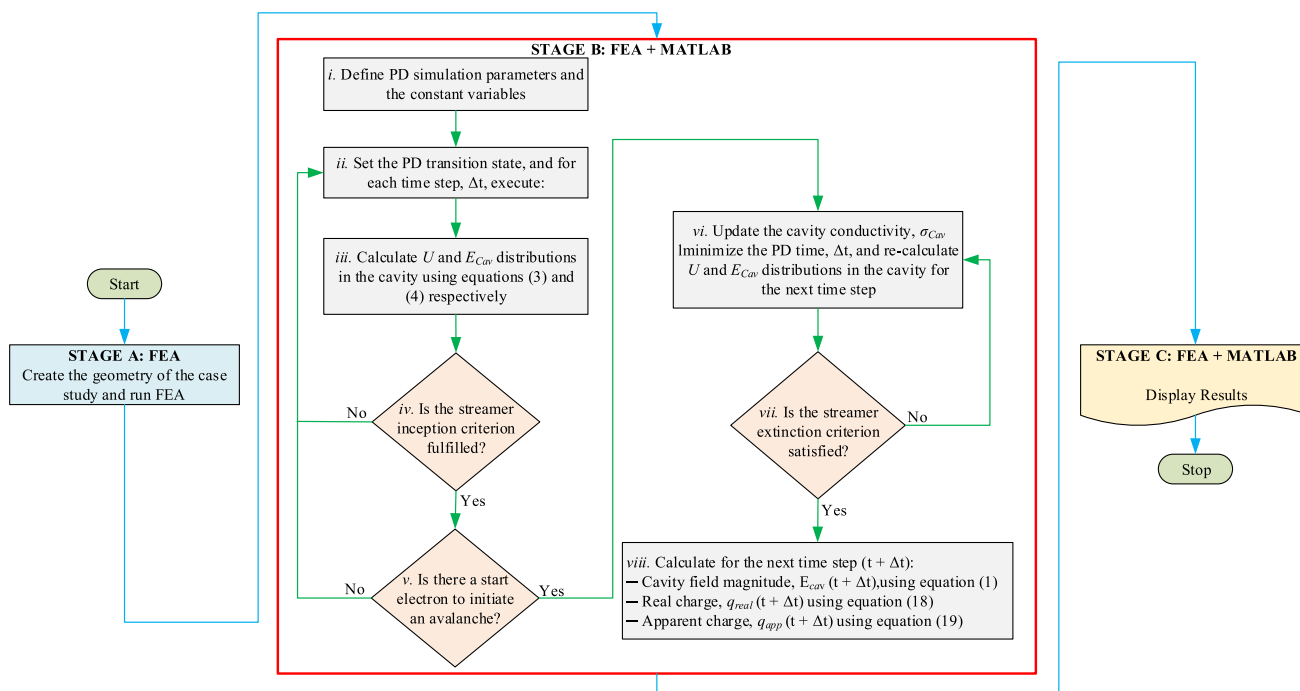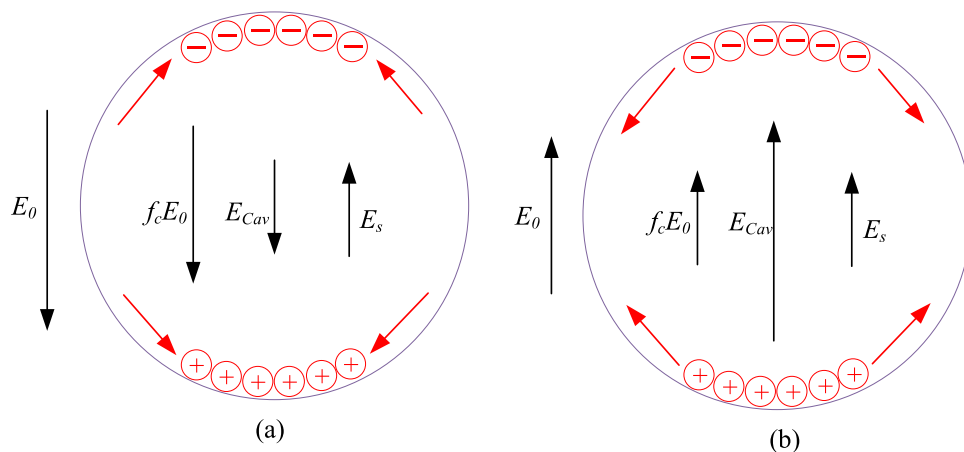

(a)   (b)

Fig. 2 Flow chart for PD simulation

the last discharge, and ξ is a proportionality constant that describes the fraction of q in a de-trappable condition.

Owing to the variation in permittivity of the surrounding material and the gas trapped inside the cavity, the applied field, E_0, is multiplied by a dimensionless field enhancement factor, f_c, to step up the local field inside the cavity. The value of f_c is obtained using the expression [65]:

$$f_c = \frac{K\varepsilon_{r,\text{surf}}}{1 + (K-1)\varepsilon_{r,\text{surf}}} \tag{11}$$

where K is a parameter that depends on the cavity geometry and $\varepsilon_{r,\text{surf}}$ is the relative permittivity of the dielectric material. K is given by [65]:

$$K = \begin{cases} \sim 1 & a/b \ll 1 \\ 3 & a/b = 1 \\ \sim 4a/b & 1 < a/b < 10 \end{cases} \tag{12}$$

where b and a are the geometrical axes of an ellipsoidal cavity perpendicular and parallel, respectively, to E_0. Since the insulation-cavity considered in this work is of spherical cross-sections (i.e. $a = b$), the value of K used is 3.

After a PD event, aside the Laplacian field, $f_c E_0$, a second component of the electric field within the cavity is the field, E_s, and is due to charges on the cavity wall from previous PD activity. Both fields ($f_c E_0$ and E_s) combine to form the net cavity electric field, E_{cav} (t). Figure 1 demonstrates the movement of trapped charges within the cavity due the
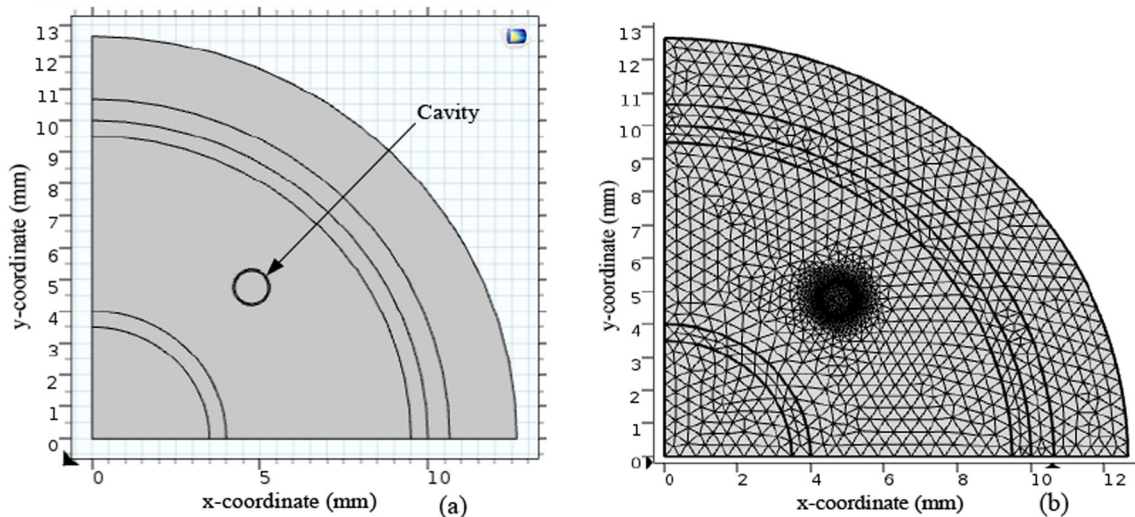
Fig. 3 Case study: **a** 2D geometry of the cable section with a cavity parallel. **b** Meshed pattern of the PD system

applied field. When the direction of E_{cav} (which is the same as $f_c E_0$) is opposed by Poison's type field (E_s), the liberated charges travel along the orientation of $f_c E_0$ and become more compact at the bottom of the cavity surface (Fig. 1a). As the direction of E_0 changes, the directions of E_{cav} and E_s become the same as shown in Fig. 1b. At this instant, charges of opposite polarity may drift through or propagate along the surface of the cavity, resulting in charge recombination [9, 65]. This process reduces the surface charge density and is thought to be the principal source of charge decay in the air-filled cavity.

2.2.3 The PD Process

The possibility of a PD owing to the presence of a seed charge in the cavity is believed to be a function of the time step and the total electron generation rate, $N_{e,tot}$ (t), when no PD activity occurs. At first, the likelihood of a seed electron, given that the magnitude of the electric field strength in the cavity is higher than the inception value, $P(t)$, at each time step, is calculated from [9]:

$$P(t) = 1 - \int_{t_{PD}}^{t_{PD}+t} N_{e,\,tot}(\tilde{t})\, d\tilde{t} \tag{13}$$

To ascertain the availability of electron at a particular time step, a randomly generated number R (between 0 and 1) is compared with $P(t)$. If $P(t) > R$, the presence of an electron is ascertained at that time step; else, the time is increased by a time step before a discharge occurs, and field magnitudes and parameters of media are calculated and updated.

2.2.4 Cavity Conductivity

The discharge inside the cavity is dynamically modelled by switching the cavity's state from non-conducting to conducting. The initial value of the cavity conductivity, σ_{cav0}, is increased to its highest value. Once the peak cavity conductivity, σ_{cav_max}, is reached, the cavity field, E_{cav} (t), at any instantaneous time keeps dropping, and the discharge finally quenches at a certain stage when E_{cav} (t) < E_{ext} [9]. σ_{cav_max} is calculated using formula (14–15):

$$\sigma_{cav\_max} = \alpha e^2 N_e \lambda_e \Big/ m_e c_e \tag{14}$$

$$N_e = \frac{q_{max}}{4/3\pi\, e\, r_{cav}^3} \tag{15}$$

where α denotes the electron energy distribution, λ_e is the electron's mean free path, m_e is the mass of the electron, c_e represents the thermal velocity of the electron, r_{cav} is the cavity radius, q_{max} represents the maximum charge magnitude, and N_e corresponds to the density of the electrons.

2.2.5 Charge Decay

At the end of each discharge, free charges deposited on the cavity wall decay before the next PD event. The charges produced might decay through charge neutralization, ion drift or surface conduction. The surface conductivity, σ_{surf}, is dependent upon the temperature and the field strength polarity of the cavity surface. When the direction of the applied field changes, σ_{surf} (see Figure 1b) is enhanced from its original value, σ_{surf0}, to model the movement of charges due to conduction within the surface of the cavity [8, 9]. Assuming a constant cavity temperature, the surface charge, σ_{surf} (t),

Table 1 PD simulation parameters [9]

Symbol	Parameter	Values
f	Frequency of applied voltage	50 Hz
U	Highest magnitude of the applied voltage	11 kV
r_{cav}	Radius of cavity	0.5 mm
σ_{cav_0}	Initial cavity conductivity	1×10^{-100} S m^{-1}
σ_{surf0}	Initial cavity surface conductivity	0 S m^{-1}
σ_{surf}	Cavity surface conductivity	S m^{-1}
$(\rho/p)_0$	Reduced gas density, air	1×10^{-5} kg^{-1} Pa^{-1} m^{-3}
$C_{rad}\,\psi_{rad}$	Radioactive quantum flux density and reduced radiative cosmic	2×10^6 kg^{-1} s^{-1}
$(E/p)_{cr}$	Gas ionization constant	2.42 V m^{-1} Pa^{-1}
ε_0	Vacuum permittivity	8.854×10^{-12}
γ	Streamer propagation factor	0.35
n	Gas ionization constant, air	0.5
B	Gas ionization parameter, air	8.6 Pa$^{1/2}$ m$^{1/2}$
T	Initial temperature of the cavity	27 K
p	Initial pressure of the cavity	9.5 kPa
ξ_+	Positive-charged surfaces de-trapping factor	0.95
ξ_-	Negative-charged surfaces de-trapping factor	1
τ_{dec}	Effective values of the time decay parameter	2 ms
v_0	Photon frequency fundamental value	1×10^{14} Hz
Φ_{dt}	Work function effective de-trapping value	1.29 eV
k_b	Boltzmann constant	8.617×10^{-5} eV K^{-1}
Δt_1	Time step before PD	0.04×10^{-3} s
Δt_2	Time step during PD	$0.0001 \times (1/f)$ s
E_{cav}	Cavity field	kV m^{-1}
E_{inc}	Inception field	kV m^{-1}
E_{ext}	Extinction field	kV m^{-1}

Table 2 Summary of PD simulation conditions [32]

No	PD system		Simulation
	Cavity radius	Conductivity of cavity surface	
1	0.4 mm, 0.8 mm, 1.2 mm, 1.6 mm	PD system is modelled without the cavity surface	PD as a function of cavity radius
2	0.5 mm	1×10^{-13} S m^{-1}, 9×10^{-13} S m^{-1} 2×10^{-11} S m^{-1}	PD as a function of the conductivity of the cavity surface

decays at each time step and is simulated using:

$$\sigma_{surf}(t) = \sigma_{surf0} \exp(\alpha|E_{cav}(t)|) \tag{16}$$

Since the cavity field, E_{cav}, is understood to be the summation of the electric field in the cavity produced by the surface charge distribution from the previous PD event and the enhanced applied field, E_{cav0}, and, E_s, then the instantaneous value of E_s is obtained from [8, 9]:

$$E_s(t) = E_{cav}(t) - f_c E_0(t) \tag{17}$$

2.2.6 Charge Magnitudes

FEA is utilized to access the current density needed for the computation of the PD charge magnitudes. Once this quantity is calculated, it is integrated over specific regions over time in order to obtain the transient current $I(t)$ flowing in the discharging system. For each PD event, the apparent and real charge magnitudes are calculated by integrating $I(t)$ through the ground electrode and cavity centre, respectively, over the discharge time interval [9]:

$$q_{real} = \int_{t_{inc}}^{t_{ext}} \int_{S_{cav}} \vec{J}(t).\,d\vec{S}\,dt \tag{18}$$

$$q_{app} = \int_{t_{inc}}^{t_{ext}} \int_{S_{G\,Electr}} \vec{J}(t).\,d\vec{S}\,dt \tag{19}$$

where t_{inc} and t_{ext} are the PD inception and extinction time, respectively, $S_{G\,Electr}$ and S_{cav} are ground electrode and surface of the cavity, respectively, dt is the time integration differential, and d $\vec{S}$ explains an infinitesimal area over which the field flows. Figure 2 depicts the flowchart for FEA modelling of PD.
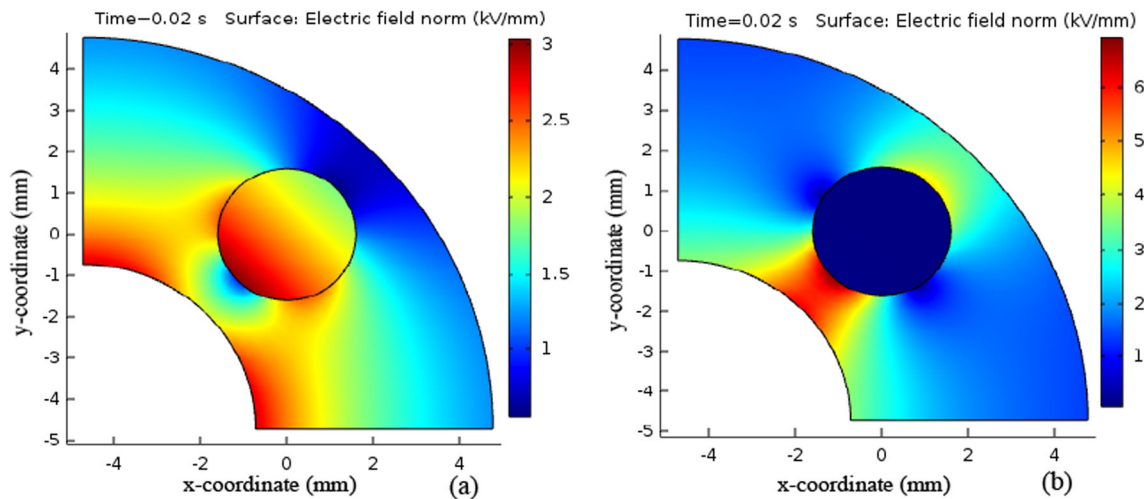
Fig. 4 The variation of electric field across the discharging PD model **a** before initial PD activity and **b** immediately after the PD activity for 1.6 mm cavity

3 Case of Study

In this work, the case study's geometry alongside a representation of its mesh is shown in Fig. 3. Its configuration is the same as that in [3], with the cavity situated right at the middle (x_axis = 3.34 mm, y_axis = 5.10 mm) of the insulation bulk. The PD model and free parameters are, respectively, listed in Tables 1, and 2. Simulations are executed considering a stressing period between 0 and 0.5 h. Because the authors were unable to measure the free parameters of the case study in this research, they were taken from the test arrangement in [66, 67] but with slight adjustments. It should be noted that the adjustments were achieved through extrapolations involving the geometrical and material parameters of the test and case models, respectively. The results of those adjustments are presented in Table 1. Such adjustments are critical in PD simulations and are carried to ensure a close agreement between simulation and measurements. PD is simulated under different conditions of cavity radius and cavity surface conductivity listed in Table 2. At the beginning of each condition, it is considered a virgin cavity without previous PD activity. A summary of the PD simulation conditions performed in this paper is therefore presented in Table 2. The magnitude of the electric field strength inside the cavity is considered homogeneous; however, it changes with time owing to sinusoidal excitation during the simulation process; the magnitudes of the inception and extinction fields are determined for each PD event.

The PD model, which was developed in COMSOL, is summarized as follows:

i. The magnitude of the electric field strength across the cavity is lower than the magnitude of the ignition field before the occurrence of a PD. The scalar potential and the electric field magnitudes can be determined using the field Eqs. (1) and (3) in COMSOL as described in Sect. 2.1;

ii. If the streamer inception condition is satisfied, the second inception pre-requisite is modelled using Eqs. (4)–(10), to check for the occurrence of PD during the subsequent time step using Eq. (13);

iii. Once the PD inception conditions are fulfilled, the time step is reduced, and the initial surface conductivity of the cavity is enhanced to a higher magnitude defined by Eq. (16);

iv. Using Eqs. (1) and (3), the electric field strength and the electric scalar potential field across the entire discharging sub-domain are recalculated until the local electric field magnitude at the cavity centre recedes below the quenching field value defined by Eq. (5); and

v. When the discharge process reaches the streamer quenching condition, the time step is reset to a higher value, and the apparent and real charges are estimated using Eqs. (18) and (19) throughout the time interval of the PD activity.

4 Results and Discussion

The activity of sustained PD in a cavity within the insulation system is modelled and analysed under different cavity sizes and surface conductivity. The associated PD parameters such as the number of PDs per cycle, real charge and inception field were investigated. Alongside the field distribution in the case study, the PD outputs were also seen to match both the simulated and experimental data in [10, 14, 67]. In those papers, the implemented model, presented in Fig. 2, was validated
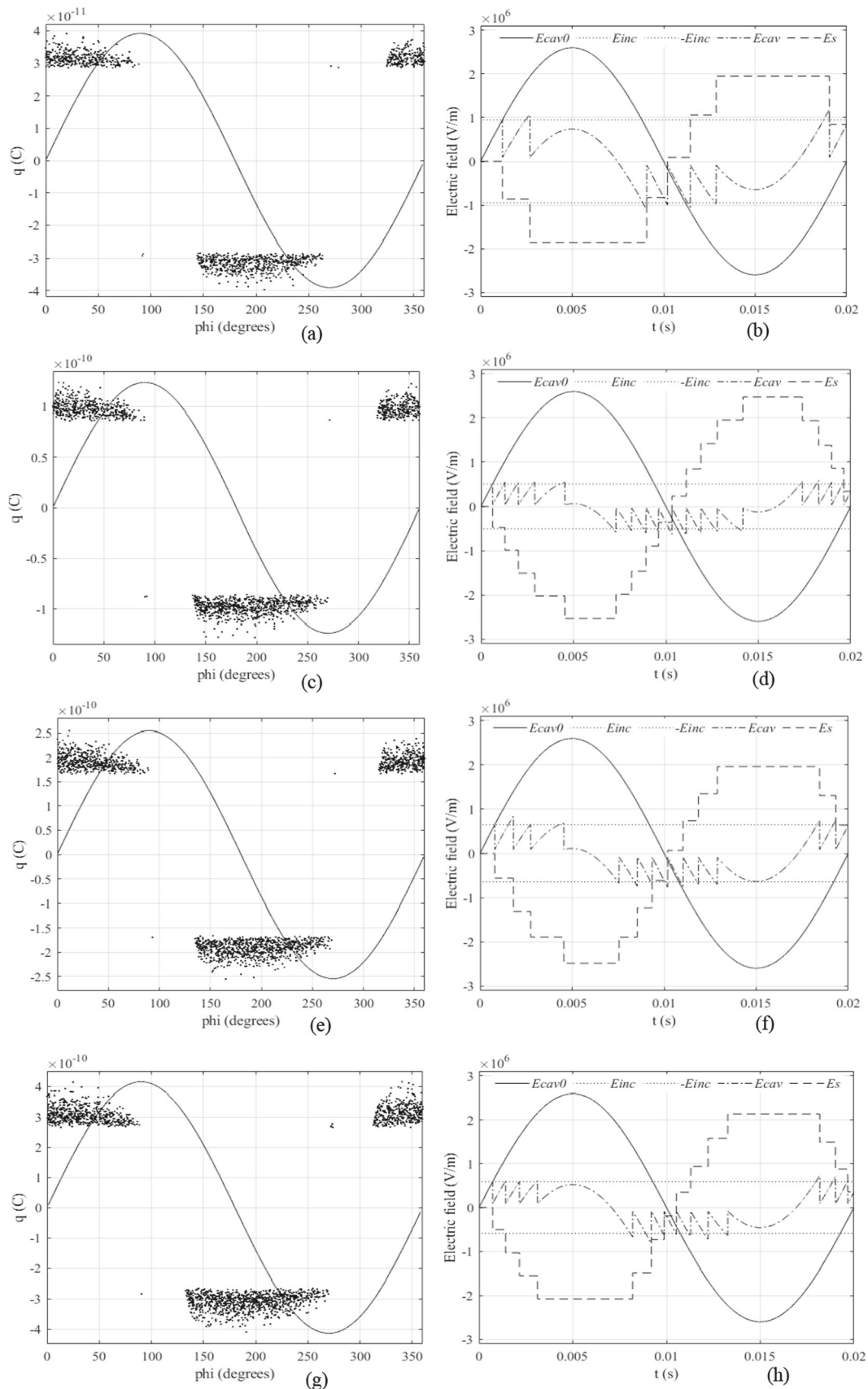
Fig. 5 PRPD patterns and electric fields for different cavity radius, $r_{cav} = 0.4$ mm: (**a**, **b**); $r_{cav} = 0.8$ mm: (**c**, **d**); $r_{cav} = 1.2$ mm: (**e**, **f**); $r_{cav} = 1.6$ mm: (**g**, **h**), simulated at 0–0.5 h, $\sigma_{suf} = 0$

Table 3 Summary of PD quantities for different cavity diameters

Item	Cavity radius, r_{cav} (mm)			
	0.4	0.8	1.2	1.6
q_{max} (pC)	48.26	180.44	263.43	**422.17**
q_{mean} (pC)	38.93	102.78	224.38	**357.68**
q_{min} (pC)	28.03	49.808	161.50	**260.18**
E_{cav} (kV m^{-1})	**4.02**	3.13	2.73	2.50
E_{inc} (kV m^{-1})	**947.08**	737.03	643.97	588.49
E_{ext} (kV m^{-1})	86.21	86.21	86.21	86.21
Number of PDs/cycle	8.72	11.91	13.87	**15.50**

Bold values indicate the highest values of the items considered under different simulation conditions

because of the good agreement between simulation results and experimental measurements.

4.1 Electric Field

Figure 4a and b depicts the variation of electric field across the geometry of the case study before and just after a discharge event, respectively. From Fig. 4a, the electric field strength reaches its maximum inside the cavity, specifically, at the dielectric-cavity boundary nearest to the HV conductor. PD charges propagate from this boundary along the straight path, crossing the cavity, towards the cavity wall closest to the ground conductor. When a PD occurs, the cavity field reduces drastically below the inception field ($E_{cav} < E_{inc}$) as illustrated in Fig. 4b. At this stage, there is a delay between the Laplacian field established by the resultant field inside the cavity and the HV source. The variation in field strengths in both stages is due to the changes in material properties.

4.2 Effect of Cavity Radius on PD

To investigate the impact of cavity size on sustained PD activity, simulations were implemented considering different cavity radius as it is shown in Table 2. Figure 5 depicts the obtained PRPD distributions and the typical electric field strength distributions per cycle for this case study. Statistical data from simulation results are provided in Table 3. In Figs. 5a, c, e and 5(g), it can be observed that all of the PRPD patterns exhibit "turtle-like" distributions. Despite the appearance of large PD pulses (positive and negative) in each half cycle, their phase distributions remain symmetrical. The number of PDs per cycle rises as cavity size increases, which can be ascribed to a faster electron production rate inside the cavity. Furthermore, the real PD charge magnitude increases with greater cavity radius, which is explained by a long streamer propagation path. Referring to values in Table 3, the peak values of number of PDs per cycle and the PD magnitude were found to be approximately 15.50 and

422.17 pC respectively in the cavity with radius of 1.6 mm. When these results are compared to that of a cavity with radius 0.4 mm, it can be seen that the number of PDs per cycle and the maximum PD charge magnitude have risen by 43.74% and 88.57%, respectively, when the radius increases to 1.6 mm.

In the same way, it was observed that while the streamer inception field magnitude increases as the cavity size becomes greater, the PD extinction field magnitude remains constant at any cavity radius. The change in inception field is mainly due to the variations in the properties of trapped cavity gas. However, it can be observed that the field magnitude of the cavity reduces as the cavity increases in size. The maximum cavity field magnitude obtained was 4.02 kV m^{-1} within the smallest cavity, 0.4 mm radius. With this value, the magnitude of the cavity field strength increased by 37.81% as compared to the 1.6 mm radius cavity. As the cavity size becomes larger, the very first phase of PD event is brought forward (see Fig. 5g). Although the average magnitude of PD charge and the number of PDs per cycle have risen due to increase in the cavity size, and the PRPD structure remains almost uniform, similar to a "turtle-like" pattern. As it is shown in Fig. 5, the PD pulses are distributed in the phases in such a way that rounded hemispheres, like the shell of a turtle, are obtained. This is because the dispersion between the values of the magnitudes of the pulses is low, and the de-trapping work function and pressure remain constant along all the simulations.

4.3 PD as a Function of Cavity Surface Conductivity

Figure 6 depicts PRPD plots from prolonged PD simulations under different conditions of cavity wall conductivity. With a streamer inception field magnitude of 871.37 kV mm^{-1}, the distribution of the PRPD pattern in Fig. 6a also exhibits a "turtle-like" structure very similar to those discussed in Fig. 5a, c, e, g. This is due to the cavity surface conductivity having a negligible impact on the cavity's sustained
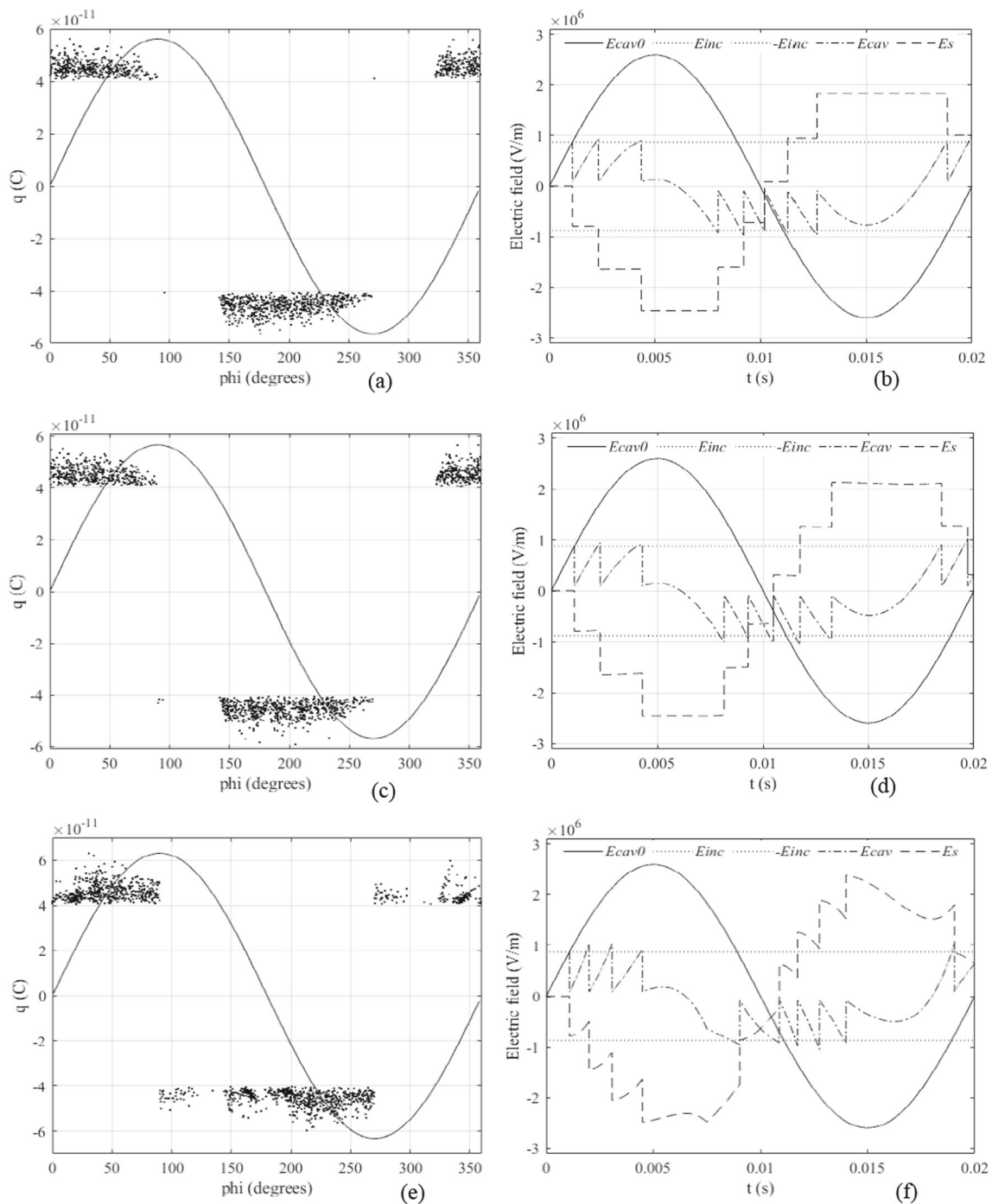
Fig. 6 PRPD patterns and electric fields for different cavity surface conductivity, $\sigma_{\text{suf1}} = 1 \times 10^{-13}$ S m^{-1} (**a, b**); $\sigma_{\text{suf2}} = 2 \times 10^{-11}$ S m^{-1}: (**c, d**); $\sigma_{\text{suf3}} = 3 \times 10^{-11}$ S m^{-1}: (**e, f**), simulated at 0–0.5 h, $r_{\text{cav}} = 0.5$ mm

PD activity. According to Table 4, when the cavity surface conductivity reaches 1×10^{-13} S m^{-1}, the maximum PD magnitude and number of PDs per cycle are approximately 58.91 pC and 9.73, respectively. Although the stated peak PD charge amplitude is the same as that of the cavity with surface conductivity of 9×10^{-13} S m^{-1}, and its magnitude is reduced by 6.36% when compared to the corresponding

case with cavity surface conductivity of 2×10^{-11} S m^{-1}. Similarly, number of PDs per cycle is reduced by 7.25% considering the earlier comparison.

As the conductivity of the surface wall is increased to 9×10^{-13} S m^{-1} and 2×10^{-11} S m^{-1}, the PRPD pattern distribution changes from "turtle-like" to "wing-like" as brought in Fig. 6c and e because in both, the dispersion of PD charge

Table 4 Summary of PD quantities for different cavity surface conductivity

Item	Cavity surface conductivity, σ_{suf} (S m^{-1})		
	1×10^{-13}	9×10^{-13}	2×10^{-11}
q_{max} (pC)	58.91	58.91	**62.91**
q_{mean} (pC)	51.10	**51.17**	48.47
q_{min} (pC)	40.50	40.50	40.90
E_{cav} (kV.m^{-1})	3.69	3.69	3.69
E_{inc} (kV.m^{-1})	871.37	871.37	871.37
E_{ext} (kV.m^{-1})	86.21	86.21	86.21
Number of PDs/cycle	9.73	9.84	**10.49**

Bold values indicate the highest values of the items considered under different simulation conditions

magnitudes and the maximum value of PD charge, increase with the conductivity of the surface wall. Among Fig. 6a, c and e, the highest number of PDs per cycle and the maximum PD charge magnitude were found to appear in Fig. 6f and e, respectively. The electric field strength magnitude produced by the surface charge distribution and the number of PDs per cycle reach their maximum values when the cavity surface conductivity reaches 2×10^{-11} S m^{-1}. Such outcomes are anticipated, owing to the ability of the cavity surface conductivity, 2×10^{-11} S m^{-1}, to contribute in the generation of higher charge (electron) in the discharging cavity. Similarly, the PRPD patterns exhibit a sort of symmetrical distribution in the various half-cycles. Despite the changes in structures of PD patterns seen in Fig. 6a, c, e, the local, streamer inception and extinction fields, respectively, remains constant within the cavity across all values of cavity surface conductivity.

5 Conclusion

A FEA-based non-deterministic model was employed to study the sustained PD activity in an air-filled spherical cavity within the insulation of an MV XLPE cable. The experimental results as reported in previous studies are in agreement with the simulation results. The discharge analysis revealed that the PRPD patterns and PD statistical quantities vary for each simulation condition. The number of PDs per cycle and their magnitudes were observed to increase as the conductivity of the cavity surface and the cavity size increased. In addition, it was observed that the PD activity increases for both, due to a larger cavity and cavities with greater surface conductivity. The greatest PD magnitude, 477.17 pC, and highest PD number per cycle, 15.50, were obtained in the cavity with 1.6 mm radius. As compared to the same

values in a smaller cavity (0.4 mm in radius), these numbers represent increases of 88.57% and 43.74%, respectively. Furthermore, the influence of cavity size on sustained PD activity was investigated and simulations with varying cavity dimensions were run. The results show that all PRPD patterns have "turtle-like" distributions. Despite the appearance of significant positive and negative PD pulses in each half cycle, their phase distributions remain symmetrical. The number of PDs per cycle rises as cavity size increases, which can be ascribed to a larger electron production rate inside the cavity. Furthermore, the size of the apparent PD charge grows by increasing the cavity radius, which is accounted by a lengthy streamer propagation path. Similarly, the approximate values for the PD number per cycle and the highest PD magnitude are 10.49 and 62.91 pC, respectively, as obtained for the highest cavity surface conductivity value of 2×10^{-11} S m^{-1}. The stated cavity conductivity value translates to a 6.36% and 7.25% increase in the number of PD per cycle and the peak PD charge magnitude, and when compared to similar values, the cavity surface conductivity corresponds to 1×10^{-13} S m^{-1}. These findings are explained by the "wing-like" distribution of the PD patterns. The results of electric field distributions and their PRPD pattern as presented in this study can be utilized in the power industry to determine the status of vital HV apparatus, and also for implementing diagnosis and prognosis studies in order to minimize equipment failure and outages.

References

1. James, R.E.; Su, Q.: Condition assessment of high voltage insulation in power system equipment, (2008). https://doi.org/10.1049/PBPO053E.
2. Rodríguez-Serna, J.M.; Albarracín-Sánchez, R.; Dong, M.; Ren, M.: Computer simulation of partial discharges in voids inside epoxy resins using three-capacitance and analytical models. Polymers (Basel). (2020). https://doi.org/10.3390/polym12010077
3. Musa, U.; Mati, A.A.; Mas'ud, A.A.; Shehu, G.S.; Albarracin-Sanchez, R.; Rodriguez-Serna, J.M.: Modeling and analysis of

electric field variation across insulation system of a MV power cable, 3rd Int. Conf. Electr. Commun. Comput. Eng. ICECCE 2021. (2021). https://doi.org/10.1109/ICECCE52056.2021.9514224.

4. Borghei, M.; Ghassemi, M.; Finite element modeling of partial discharge activity within a spherical cavity in a solid dielectric material under fast, repetitive voltage pulses, in: 2019 IEEE Electr. Insul. Conf. EIC 2019, 2019. https://doi.org/10.1109/EIC43217.2019.9046525.

5. Rodríguez-Serna, J.M.; Albarracín-Sánchez, R.; Mas'ud, A.A.: Finite-element-analysis models for numerical simulation of partial discharges in spherical cavities within solid dielectrics: a review and a novel method, High Volt. (2020). https://doi.org/10.1049/hve.2019.0392.

6. Borghei, M.: Ghassemi, M.: Partial discharge analysis under high-frequency, fast-rise square wave voltages in silicone gel: a modeling approach, Energies. (2019). https://doi.org/10.3390/EN12234543.

7. Gouda, O.E.; ElFarskoury, A.A.; Elsinnary, A.R.; Farag, A.A.: Investigating the effect of cavity size within medium-voltage power cable on partial discharge behaviour. IET Gener. Transm. Distrib. (2018). https://doi.org/10.1049/iet-gtd.2017.1012

8. Niemeyer, L.: A generalized approach to partial discharge modeling. IEEE Trans. Dielectr. Electr. Insul. (1995). https://doi.org/10.1109/94.407017

9. Gutfleisch, F.; Niemeyer, L.: Measurement and simulation of PD in Epoxy voids. IEEE Trans. Dielectr. Electr. Insul. (1995). https://doi.org/10.1109/94.469970

10. Borghei, M.; Ghassemi, M.; Rodriguez-Serna, J.M.; Albarracin-Sanchez, R.: A finite element analysis and an improved induced charge concept for partial discharge modeling. IEEE Trans. Power Deliv. 36, 2570–2581 (2021). https://doi.org/10.1109/TPWRD.2020.2991589

11. Ragusa, A.; Sasse, H.; Duffy, A.P.: 3D model of partial discharge in defects with different sizes and positions in power cable for distribution and transmission networks. IET Sci. Meas. Technol. (2020). https://doi.org/10.1049/iet-smt.2019.0351

12. Illias, H.; Chen, G.; Lewin, P.: Partial discharge behavior within a spherical cavity in a solid dielectric material as a function of frequency and amplitude of the applied voltage. IEEE Trans. Dielectr. Electr. Insul. (2011). https://doi.org/10.1109/TDEI.2011.5739447

13. Morsalin, S.; Phung, B.T.; Cavallini, A.: Measurement and modeling of partial discharge arising from different cavity geometries at very low frequency. IEEE Trans. Dielectr. Electr. Insul. (2020). https://doi.org/10.1109/TDEI.2020.008668

14. Illias, H.A.; Tunio, M.A.; Bakar, A.H.A.; Mokhlis, H.; Chen, G.: Partial discharge phenomena within an artificial void in cable insulation geometry: experimental validation and simulation. IEEE Trans. Dielectr. Electr. Insul. 23, 451–459 (2016). https://doi.org/10.1109/TDEI.2015.005155

15. Illias, H.A.; Chen, G.; Lewin, P.L.: Partial discharge within a spherical cavity in a dielectric material as a function of cavity size and material temperature. IET Sci. Meas. Technol. 6, 52–62 (2012). https://doi.org/10.1049/IET-SMT.2011.0091

16. Chen, Y.; Hui, B.; Cheng, Y.; Hao, Y.; Fu, M.; Yang, L.; Hou, S.; Li, L.: Failure investigation of buffer layers in high-voltage XLPE cables. Eng. Fail. Anal. (2020). https://doi.org/10.1016/J.ENGFAILANAL.2020.104546

17. Edin, H.: Partial discharges studied with variable frequency of the applied voltage, PhD dissertation, KTH, Stockholm, Sweden (2001).

18. Forssén, C.; Edin, H.: Partial discharges in a cavity at variable applied frequency part 2: measurements and modeling. IEEE Trans. Dielectr. Electr. Insul. 15, 1610–1616 (2008). https://doi.org/10.1109/TDEI.2008.4712664

19. Mas'ud, A.: Experimental investigation of different cavity arrangements in the high voltage solid insulation systems, Yanbu J. Eng. Sci. 19: 78–85. (2022) https://doi.org/10.53370/001C.35686.

20. Callender, G.; Golosnoy, I.O.; Rapisarda, P.; Lewin, P.L.: Critical analysis of partial discharge dynamics in air filled spherical voids. J. Phys. D. Appl. Phys. (2018). https://doi.org/10.1088/1361-6463/AAAE7C

21. Rodríguez-Serna, J.M.; Albarracín-Sánchez, R.: Numerical simulation of temperature and pressure changes due to partial discharges in spherical cavities within solid dielectrics at different ageing conditions. Energies (2019). https://doi.org/10.3390/en12244771

22. Akram, S.; Wang, P.; Nazir, M.T.; Zhou, K.; Bhutta, M.S.; Hussain, H.: Impact of impulse voltage frequency on the partial discharge characteristic of electric vehicles motor insulation. Eng. Fail. Anal. (2020). https://doi.org/10.1016/J.ENGFAILANAL.2020.104767

23. Rodriguez-Serna, J.M.; Albarracin-Sanchez, R.: Simulation of polymeric insulators ageing induced by the impact energy of electrons during partial discharge activity, 2021 IEEE Texas Power Energy Conf. TPEC 2021. (2021). https://doi.org/10.1109/TPEC51183.2021.9384986.

24. Wang, L.; Cavallini, A.; Montanari, G.C.; Testa, L.: Evolution of PD patterns in polyethylene insulation cavities under AC voltage. IEEE Trans. Dielectr. Electr. Insul. 19, 533–542 (2012). https://doi.org/10.1109/TDEI.2012.6180247

25. Montanari, G.C.; Cavallini, A.; Testa, L.; Serra, S.; Dissado, L.A.: Model of ageing inception and growth from microvoids in polyethylene-based materials under AC voltage, 29–32. (2009) https://doi.org/10.1109/CEIDP.2008.4772903.

26. G. Callender, P. Rapisarda, P.L.; Lewin, Investigation of void erosion on partial discharge activity using simulation, Proc. 2016 IEEE Int. Conf. Dielectr. ICD 2016. 2 (2016). https://doi.org/10.1109/ICD.2016.7547762.

27. Tanmaneeprasert, T.; Lewin, P.L.; Callender, G.: Measuring and simulating partial discharge activity in a spherical cavity during electrical ageing processes, 2018 IEEE 2nd Int. Conf. Dielectr. ICD 2018. (2018). https://doi.org/10.1109/ICD.2018.8468433.

28. Lv, Z.; Rowland, S.M.; Chen, S.; Zheng, H.; Iddrissu, I.: Evolution of partial discharges during early tree propagation in epoxy resin. IEEE Trans. Dielectr. Electr. Insul. (2017). https://doi.org/10.1109/TDEI.2017.006731

29. Mazzanti, G.; Montanari, G.C.; Civenni, F.: Model of inception and growth of damage from microvoids in polyethylene-based materials for HVDC cables part 2: parametric investigation and data fitting. IEEE Trans. Dielectr. Electr. Insul. 14, 1255–1263 (2007). https://doi.org/10.1109/TDEI.2007.4339486

30. Feng, X.; Xiong, Q.; Gattozzi, A.L.; Hebner, R.E.: Partial discharge experimental study for medium voltage DC cables. IEEE Trans. Power Deliv. 36, 1128–1136 (2021). https://doi.org/10.1109/TPWRD.2020.3002508

31. Liu, Q.; Zheng, S.S.; Zhang, Q.; Ying, H.Y.: Experimental study on UHF pattern of partial discharges in transformer bushings, ICHVE 2016–2016 IEEE Int. Conf. High Volt. Eng. Appl. (2016). https://doi.org/10.1109/ICHVE.2016.7800743

32. Zhang, J.; Xu, M.; Guo, Y.; Zhang, K.; Liu, H.; Zhao, X.: Experimental research on partial discharge of high voltage direct current. J. Phys. Conf. Ser. (2021). https://doi.org/10.1088/1742-6596/1865/2/022026

33. Khan, Q.; Refaat, S.S.; Abu-Rub, H.; Toliyat, H.A.: Partial discharge detection and diagnosis in gas insulated switchgear: state of the art. IEEE Electr. Insul. Mag. 35, 16–33 (2019). https://doi.org/10.1109/MEI.2019.8735667

34. Whitehead, S.: Dielectric Breakdown of Solids. Clarendon Press, 1951. https://www.abebooks.com/first-edition/Dielectric-Breakdown-Solids-Whitehead-Oxford-Clarendon/30952810208/bd (accessed September 29, 2022).

35. Callender, G.; Tanmaneeprasert, T.; Lewin, P.L.: simulating partial discharge activity in a cylindrical void using a model of plasma dynamics. J. Phys. D. Appl. Phys. (2019). https://doi.org/10.1088/1361-6463/AAEDF0

36. Pan, C.; Chen, G.; Tang, J.; Wu, K.: Numerical modeling of partial discharges in a solid dielectric-bounded cavity: a review. IEEE Trans. Dielectr. Electr. Insul. **26**, 981–1000 (2019). https://doi.org/10.1109/TDEI.2019.8726048

37. Morrow, R.; Lowke, J.J.: Streamer propagation in air. J. Phys. D. Appl. Phys. **30**, 614–627 (1997). https://doi.org/10.1088/0022-3727/30/4/017

38. Tanmaneeprasert, T.; Lewin, P.L.; Callender, G.: Analysis of degradation mechanisms of silicone insulation containing a spherical cavity using partial discharge detection. 2017 IEEE Electr. Insul. Conf. EIC **2017**, 233–236 (2017). https://doi.org/10.1109/EIC.2017.8004633

39. Pedersen, A.: Partial discharges in voids in solid dielectrics. An alternative approach, in Conference on electrical insulation dielectric phenomena–annual report 1987, pp. 58–64. (1987) https://doi.org/10.1109/CEIDP.1987.7736534.

40. Chan, J.C.; Duffy, P.; Hiivala, L.J.; Wasik, J.: Partial discharge. VIII. PD testing of solid dielectric cable. IEEE Electr. Insul. Mag. **7**(5), 9–16 (1991). https://doi.org/10.1109/57.93157

41. He, M. et al., Numerical modelling on partial discharge in HVDC XLPE cable, COMPEL, pp. 00–00, (2018), https://doi.org/10.1108/COMPEL-07-2017-0297.

42. Patsch, R.; and Hoof, M.: Physical modeling of partial discharge patterns, in ICSD'98. Proceedings of the 1998 IEEE 6th International Conference on Conduction and Breakdown in Solid Dielectrics (Cat. No.98CH36132), pp. 114–118. (1998) https://doi.org/10.1109/ICSD.1998.709239.

43. Hoof, M.; and Patsch, R.: A physical model, describing the nature of partial discharge pulse sequences, in Proceedings of 5th International Conference on Properties and Applications of Dielectric Materials, vol. 1, pp. 283–286 (1997) https://doi.org/10.1109/ICPADM.1997.617583.

44. Gemant, A.; Philippoff, W.: Spark gap with pre-capacitor. Z. Tech. Phys. **13**(9), 425–430 (1932)

45. Gopinath, S.; Sathiyasekar, K.: Simulation of partial discharges in solid dielectric material: a study on PD magnitudes to the parallel and. Int. J. Eng. Technol. **6**(4), 7 (2014)

46. Sabat, A.; Karmakar, S.: Simulation of partial discharge in high voltage power equipment. Int. J. Electr. Eng. Inform. **3**(2), 234–247 (2011). https://doi.org/10.15676/ijeei.2011.3.2.8

47. Kolev, N.; Darjanov, P.; Gadjeva, E. and Darjanova, D.: Partial discharge phenomena simulation using general-purpose analysis programs, in ICSD'98. Proceedings of the 1998 IEEE 6th International Conference on Conduction and Breakdown in Solid Dielectrics (Cat. No.98CH36132), pp. 149–152 (1998). https://doi.org/10.1109/ICSD.1998.709247.

48. Christina, A.J. et al.: Partial discharge modeling with increasing applied voltages across different void sizes, in 2017 4th International Conference on Advances in Electrical Engineering (ICAEE), pp. 22–25. (2017) https://doi.org/10.1109/ICAEE.2017.8255320.

49. M. Nafar, "Simulation of Partial Discharge Mechanism using EMTP," in Proceedings of the International Conference on Innovations in Electrical and Electronics Engineering (ICIEE'2012), Dubai, UAE, Oct. 2012, pp. 249–251. [Online]. Available: http://psrcentre.org/images/extraimages/18%201012188.pdf

50. Illias, H.; Chen, G.; and Lewin, P. L.: Modelling of surface charge decay in a spherical cavity within a solid dielectric material using finite element analysis, in Proceedings of the 16th International Symposium on High Voltage Engineering, Cape Town, South Africa, Aug. 2009, pp. 1246–1251. [Online]. Available: http://eprints.soton.ac.uk/id/eprint/267820

51. Gafvert, U.; Edin, H.; and Forssen, C.: Modelling of partial discharge spectra measured with variable applied frequency, in Proceedings of the 7th International Conference on Properties and Applications of Dielectric Materials (Cat. No.03CH37417),

vol. 3, pp. 839–842 (2003) https://doi.org/10.1109/ICPADM.2003.1218552.

52. Illias, H.A.; Chen, G.; and Lewin, P. L.: Partial discharge modelling in a spherical cavity within a dielectric insulation material as a function of frequency, in 2009 IEEE Electrical Insulation Conference, pp. 55–59. (2009) https://doi.org/10.1109/EIC.2009.5166323.

53. Wu, K.; Suzuoki, Y.; and Dissado, L. A.: Improved simulation model for PD pattern in voids considering effects of discharge area, in 2003 Annual Report Conference on Electrical Insulation and Dielectric Phenomena, (2003), pp. 32–35. https://doi.org/10.1109/CEIDP.2003.1254787.

54. Illias, H.; Jian, L. T.; Bakar, A. H. A.; and Mokhlis, H.: Partial discharge simulation under various applied voltage waveforms, in 2012 IEEE International Conference on Power and Energy (PECon), (2012), pp. 967–972. https://doi.org/10.1109/PECon.2012.6450358.

55. Illias, H.A.; Tunio, M.A.; Bakar, A.H.A.; Mokhlis, H.; Chen, G.: Partial discharge behaviours within a void-dielectric system under square waveform applied voltage stress. IET Sci., Measure. Technol. **8**(2), 81–88 (2014). https://doi.org/10.1049/iet-smt.2013.0018

56. Illias, H.A.; Tunio, M.A.; Mokhlis, H.; Chen, G.; Bakar, A.H.A.: Experiment and modeling of void discharges within dielectric insulation material under impulse voltage. IEEE Trans. Dielectr. Electr. Insul. **22**(4), 2252–2260 (2015). https://doi.org/10.1109/TDEI.2015.004817

57. Illias, H.; Chen, G.; Lewin, P.L.: Modeling of partial discharge activity in spherical cavities within a dielectric material. IEEE Electr. Insul. Mag. **27**(1), 38–45 (2011). https://doi.org/10.1109/MEI.2011.5699446

58. Illias, H. A.; Chen, G.; and Lewin, P. L.: Modelling of partial discharge activity in different spherical cavity sizes and locations within a dielectric insulation material, in 2009 IEEE 9th International Conference on the Properties and Applications of Dielectric Materials, (2009), pp. 485–488. https://doi.org/10.1109/ICPADM.2009.5252384.

59. Illias, H.A.; Tunio, M.A.; Mokhlis, H.; Chen, G.; Bakar, A.H.A.: Determination of partial discharge time lag in void using physical model approach. IEEE Trans. Dielectr. Electr. Insul. **22**(1), 463–471 (2015). https://doi.org/10.1109/TDEI.2014.004618

60. Illias, H. A.; Chen, G.; and Lewin, P. L.: Partial discharge behaviour within two spherical cavities in a dielectric material, in 2011 Annual Report Conference on Electrical Insulation and Dielectric Phenomena, Oct. 2011, pp. 456–459. https://doi.org/10.1109/CEIDP.2011.6232693.

61. Callender, G. Modelling partial discharge in gaseous voids, PhD, University of Southampton, Southamptom, U.K., 2018. Accessed: Jun. 07, 2019. [Online]. Available: https://eprints.soton.ac.uk/420943/

62. Illias, H. A., Chen, G. and Lewin, P. L.: The influence of spherical cavity surface charge distribution on the sequence of partial discharge events, J. Phys. D Appl. Phys. 44(24), 245202-16, (2011) https://doi.org/10.1088/0022-3727/44/24/245202.

63. Pan, C.; Tang, J.; Zeng, F.: Numerical modeling of partial discharge development process. Plasma Sci. Technol.–Basic Fundam. Mod. Appl. (2018). https://doi.org/10.5772/intechopen.79215

64. Leon-Garzon, A.R.; Dotelli, G.; Villa, A.; Barbieri, L.; Gondola, M.; Cavallotti, C.: Thermodynamic analysis of the degradation of polyethylene subjected to internal partial discharges. Chem. Eng. Sci. **180**, 1–10 (2018). https://doi.org/10.1016/j.ces.2018.01.023

65. Lei, Z.; Song, J.; Tian, M.; Cui, X.; Li, C.; Wen, M.: Partial discharges of cavities in ethylene propylene rubber insulation. IEEE Trans. Dielectr. Electr. Insul. **21**, 1647–1659 (2014). https://doi.org/10.1109/TDEI.2014.004297

66. Setayeshmehr, A.; Akbari, A.; Borsi, H.; Gockenbach, E.: On-line monitoring and diagnoses of power transformer bushings. IEEE Trans. Dielectr. Electr. Insul. **13**, 608–615 (2006). https://doi.org/10.1109/TDEI.2006.1657975

67. Tanmaneeprasert, T.: An investigation into electrical degradation mechanisms within air-filled cavities in solid dielectric materials', PhD Dissertation, University of Southampton, UK (2018).